Toward an understanding of the effect of surface roughness on instrumented indentation results

Julie Marteau, Maxence Bigerelle

Toward an understanding of the effect of surface roughness on instrumented indentation results

J. Marteau[1,*] and M. Bigerelle[2]

[1] *Laboratoire Roberval, UMR-CNRS 7337, Centre de Recherches de Royallieu, Galileo Galilei, Sorbonne Universités, Université de Technologie de Compiègne, Compiègne, France*

[2] *Laboratoire d'Automatique, de Mécanique et d'Informatique industrielle et Humaine (LAMIH), UMR-CNRS 8201, Université de Valenciennes et du Hainaut Cambrésis, Le Mont Houy, Valenciennes, France*

ABSTRACT

Performing indentation tests on rough surfaces at the microscale creates non-negligible scatter of the load–indentation depth curves and leads to an inaccurate computation of mechanical properties. In previous work, the minimization of the error between the shapes of the experimental loading curve and the shapes predicted by Bernhardt's law enabled the macrohardness of the material to be determined with accuracy and to identify a relationship between the standard deviation of the errors of shapes and the root-mean-square roughness (S_q) computed at the scale of the indentation imprint. In this paper, a semi-analytical model applied to roughness measurements is used to understand this relationship. Good agreement is found between the model results and the experimental results. Analysis of the semi-analytical model confirmed that the identified relationship is caused by the topography and not by some experimental bias and that the relevant scale for the computation of S_q is the scale of the indentation imprints (15 μm). However, the relationships found with the model and the experimental results show different slopes and y-intercepts. The y-intercept found with the numerical curves is negligible compared with the y-intercept identified with the experimental curve, which is equal to 30 nm. This indicates that even if S_q is equal to zero, the zero-point of the curve is not accurately determined by the instrumented indentation device. As for the differences in slope, these may be partly due to experimental noise and the differences of methodology of detections of first-contact for the recording of the load–displacement curves. Overestimation of the resistance of abrasion debris by the semi-analytical model may also explain the differences of slopes. However, further testing is required to confirm this hypothesis.

Address correspondence to E-mail: julie.marteau@utc.fr

Introduction

Subsurface measurements of mechanical properties are of crucial importance for linking process conditions with the obtained mechanical properties. Instrumented indentation is a popular technique for investigating the subsurface properties. However, some processes (e.g., mechanical processes, thermochemical processes) tend to induce surface roughness, thus complicating the determination of mechanical properties with instrumented indentation. Surface roughness causes the scattering of the load–indentation depth curves and thus complicates the computation of mechanical properties such as hardness and Young's modulus [1–3]. Methods have been proposed for dealing with the uncertainties caused by surface roughness [4–6]. Kim et al. [4] developed a new indentation size effect (ISE) model that separates the work needed to flatten the surface from the one required to deform the flattened surface. Guillonneau et al. [5] developed a method for minimizing displacement measurement uncertainties based on the determination of the contact depth derivative. However, understanding the influence of roughness on indentation testing and the determination of mechanical properties remains complex. The examination of surface roughness is often an issue as it can be investigated at different scales. Basically, surface topography can be decomposed into waviness (low frequencies) and micro-roughness (high frequencies). Roughness amplitude is also directly linked with the spatial window considered for the examination: More specifically, the values of the roughness parameters describing surface texture are dependent on the considered spatial window. ISO Standard 4287 [7] provides methods for general assessment of surface texture. It defines the sampling length as the "length in the x-direction used for identifying the irregularities characterizing the profile under evaluation." It is thus the distance required for an appropriate computation of the roughness parameters. Instead of computing roughness parameters using only one sampling length per profile, consecutive sampling lengths are usually used. The advised number is 5 according to ISO Standard 4288 [8].

One of the main issues of the simulation of rough contact (experimental or numerical) is thus defining the macroscopic scale at which roughness can be considered as stationary, or more specifically, representative of contact.

In previous work [6], the simultaneous treatment of the indentation curves located according to the error between their shape and that predicted by Bernhardt's law [9] enabled us to determine the material macrohardness with accuracy despite significant surface roughness. This method was tested on several different materials and surface topographies (obtained using different surface treatments) [10–13]. A relationship between the standard deviation of the errors between the indentation curve shapes and the shape predicted by Bernhardt's law and the root-mean-square roughness (S_q) computed at the scale of the indentation imprint was identified for all the studied cases (i.e., whatever the tested material or surface topography). In this paper, a semi-analytical model is applied to roughness measurements performed on Ti–6Al–4V specimens in order to study this relationship validity.

Materials and methods

In this section, all the experimental data corresponding to previous studies [6, 10–14] are summarized, even though only Ti–6Al–4V specimens ground with different grit papers are thoroughly examined in this paper. This summary includes the main characteristics of the materials, as well as the hardness and roughness measurements.

Materials and processing parameters

First, whatever the material or the examined process, all the specimens were mirror-polished.

Three studies were focused on the examination of specimens ground with an automatic device having off-centered rotating movements. Different surfaces were obtained using different grit papers with identical force and time conditions (150 N, 3 min). Grit papers having the following numbers were used: 80, 120, 180, 220, 320, 500, 800, 1000, 1200, 2400 and 4000. This procedure was applied to three different materials: AU4G aluminum-based alloy, AISI 316L austenitic stainless steel [6] and titanium-based alloy Ti–6Al–4V [10].

The surfaces of seven of the eleven Ti–6Al–4V specimens were replicated using MD-3P in order to get similar surface topography but different hardness. MD-3P (Plastiform®, France) is a replica material made of resin, powder and hardening agent for
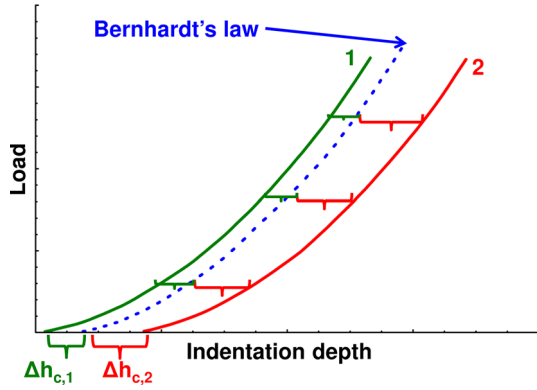
Figure 1 Schematic drawing of the meaning of Δh_c, the error between the shape of the loading curves predicted by Bernhardt's law and the shape of the experimental curves.

its polymerization at room temperature. The replicated specimens have the same morphology as the Ti–6Al–4V specimens obtained with grit papers 80, 120, 220, 500, 800, 1200 and 2400 [14].

AU4G aluminum-based alloy samples were sandblasted using 500-μm Al_2O_3 particles. Only three process parameters were varied (pressure, distance and included angle between the specimen and the nozzle). From the combination of these process parameters, four specimens were analyzed [12, 13]. Two specimens were sandblasted with a pressure of 1 bar, an included angle of 0° and a nozzle-to-specimen distance equal to either 15 cm or 30 cm. The other two specimens were made with a pressure of 0.5 bar, a nozzle-to-specimen distance of 30 cm and an included angle equal to either 0° or 30°.

Finally, AISI 316L stainless steel samples were ultrasonically shot-peened using the following process parameters: shot diameters of 1 or 2 mm, shots of 304L stainless steel or 100C6 steel, sonotrode amplitude vibration of 30, 60 or 80 μm and coverage of 100, 1000 or 10,000%. Among the different combinations, eight ultrasonically shot-peened specimens were examined [11].

All these different materials and surface treatments give a total of 52 specimens. Details of the treatments and process parameters can be found in the cited articles.

Measurement of hardness

Each specimen was tested using instrumented indentation at ambient temperature with a Berkovich tip (or a cube-corner tip for one set of samples). A maximum indentation depth of 3 μm was reached. One hundred load–displacement curves were obtained for each specimen. A constant strain rate equal to $0.05~s^{-1}$ was used. Because of the non-negligible topography of the specimens caused by the different surface treatments, there was a large scatter of the loading curves. In order to identify macrohardness despite non-negligible surface roughness, the methodology thoroughly described in [15] was applied. In this methodology, only the loading parts of the curves are kept and are pretreated in order to avoid any statistical artifacts. All the details are given in [6, 15]. In short, this methodology is based on the model proposed by Bernhardt [9], who described the relation between the load P and indentation depth h as follows:

$$P = \left\{ \alpha_1 h^2 + \alpha_2 h \right\}, \tag{1}$$

where α_1 and α_2 are constants determined by the indenter tip geometry and the material properties. This equation is modified by rewriting it using the contact depth h_c defined by Oliver and Pharr [16], the macrohardness H_0, the indentation size effect factor β, as follows:

$$P = \alpha \left(H_0 h_c^2 + \beta h_c \right). \tag{2}$$

Then, it is assumed that there is an error between Bernhardt's model and the real shape of the experimental loading curves that we will refer to as Δh_c. For the sake of clarity, Δh_c is schematically represented in Fig. 1. The following minimization was performed using the loading parts of the one hundred instrumented indentation curves:

$$\min_{H_0, \Delta h_1 \ldots \Delta h_n, \beta} \sum_{i=1}^{n} \sum_{j=1}^{p_i}$$
$$\left[P_{i,j} - \alpha \left(H_0 h_{c,j}^2 + (2H_0 \Delta h_{c,i} + \beta) h_{cj} + H_0 \Delta h_{c,i}^2 + \beta \Delta h_{c,i} \right) \right]^2, \tag{3}$$

where index j refers to a point that is part of curve i and α is a constant depending on the geometry of the indenter. Thus, in this methodology, one value of macrohardness H_0 and ISE coefficient β is identified by the minimization made on a set of curves.

Measurement of roughness

Roughness measurements were taken using either a three-dimensional tactile profilometer or an optical profilometer.

The tactile profilometer (TENCOR™ P10, KLA-TENCOR, USA) was equipped with a 2-mm tip stylus and have a vertical resolution of the nanometer order. As the examined surfaces are isotropic, thirty-two-dimensional profiles having a 5 mm length were recorded with high sampling frequency and a 200 μm/s speed.

The optical profilometer (Zygo Newview™ 7300, Zygo corp., USA) was used with 20× objective, giving a lateral accuracy equal to 71 nm and a vertical accuracy of about 3 nm. To have large surface areas, ten 348 × 262 μm areas were stitched with an overlapping percentage equal to 20%, thus giving surfaces of 1.19 × 0.891 mm described by 2176 × 1632 points. Twenty measurements were taken on each specimen.

All the measurements were rectified before the computation of the roughness parameters. Only one roughness parameter is used in this study: the root-mean-square deviation of the surface S_q (or R_q for the two-dimensional surfaces). This parameter is computed with a Gaussian high-pass filter, using different cutoff lengths in order to identify the best scale at which contact should be examined.

Semi-analytical model for numerical simulation

In order to deal with the stochastic aspect of roughness, a very large number of numerical simulations are required. Moreover, a detailed description of roughness is required. This is why a semi-analytical model is used with pavements of 256 × 256.

Rough surfaces were built using the topography measurements taken on the Ti–6Al–4V specimens ground with different grit sizes using the optical profilometer equipped with 20× objective. As indicated in "Measurement of roughness" section, twenty measurements having a size of 1.19 mm × 0.891 mm were taken on each specimen. These topography measurements were recut in order to get as many surfaces as possible for the indentation tests: 270 surfaces were obtained by specimen.

This semi-analytical model describes the contact between a rough surface and a perfectly smooth and rigid indenter. Contacts are local, i.e., they are only located at the summits of the surface and are investigated by the analysis of the geometry of the local summits. The asperities are described as cones having different angles of contact. The elastic interactions between the asperities are neglected. According to Johnson's equations of elastic–plastic indentation with a conical indenter [17], the mean pressure p_{jm} undergone by a given asperity j is:

$$p_{jm} = \frac{2}{3} Y \left(1 + \ln\left(\frac{E tan\theta_j}{3Y} \right) \right), \tag{4}$$

where Y is the elastic limit, E is the Young's modulus of the material, and θ is the attack angle, i.e., the inclination of the face of the cone to the surface.

In the examined case, a fully plastic deformation is thus considered:

$$p_m \sim 3Y \sim H \tag{5}$$

For the computation, the local areas of contact A_j are elliptic with semi-axes a_j and b_j. The local areas of contact are discretized into N elements c_{ji} ($I = 1, …, N$). The distribution of local pressure on a given asperity j is:

$$p_j(x_i, y_i) = \frac{3}{2} p_{jm} \left(1 - \left(\frac{x_i}{a_j} \right)^2 - \left(\frac{y_i}{b_j} \right)^2 \right)^{1/2} \tag{6}$$

The normal force F_j exerted on an asperity j is:

$$F_j = \sum_i c_{ji} p_i \tag{7}$$

The load carried by the summits of the rough surface is the sum of the normal forces F_j.

The numerical model is thoroughly described in [18].

The depth of the indentation test was equal to 3 μm, and a Berkovich tip was used in order to match the experimental data. A perfectly plastic behavior was chosen for the numerical simulations as the strain-hardening coefficient of Ti–6Al–4V is small. The Young's modulus E of the material is equal to 110 GPa, its Poisson's coefficient is equal to 0.3, and its elastic limit is equal to 1050 MPa. Tresca's criterion is used.

Results and discussion

Previously found results

Non-negligible surface topography induces a scatter of the instrumented indentation curves. The scatter of the instrumented indentation curves was previously examined using different materials and surface topographies (obtained with different surface treatments) [6, 10–14]. Using the methodology described in "Measurement of hardness" section, the macro-hardness H_0 was accurately identified despite the

Figure 2 Standard deviation of the errors Δh_c as a function of the root-mean-square roughness S_q (or R_q) computed with a high-pass filter and a cutoff length equal to 15 μm for all the specimens indented with a Berkovich indenter (B) and a cutoff length equal to 5 mm for the cube-corner indenter (C). The materials are AISI 316L stainless steel (316L), aluminum alloy (AU4G), titanium-based alloy Ti–6Al–4V (TA6V4), MD-3P replica material (MD-3P). The following letters correspond to processes: P for polishing, S for sandblasting and U for ultrasonic shot-peening.
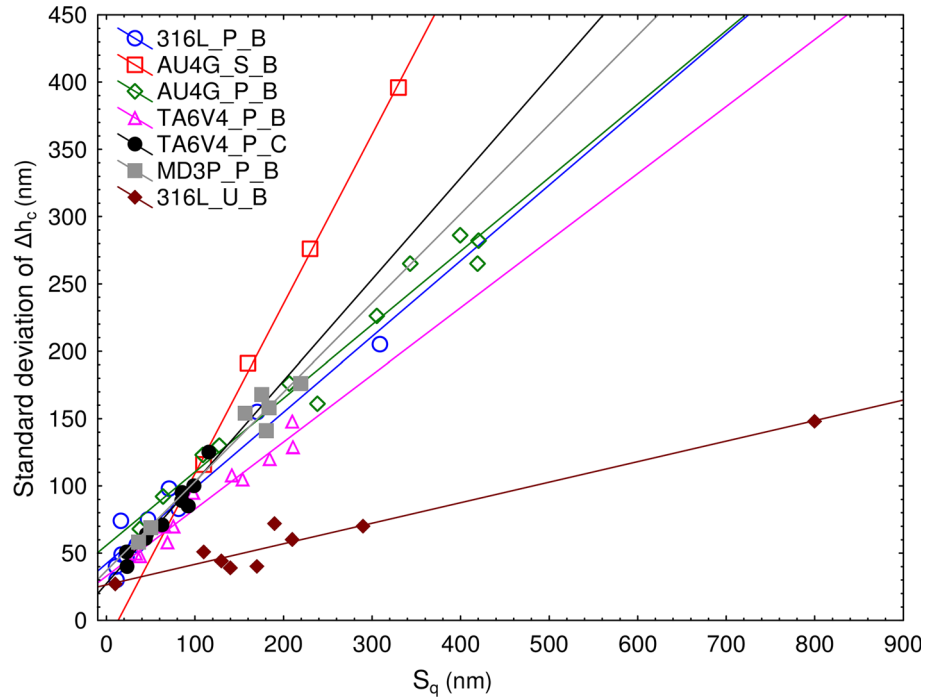
scatter of the curves through the minimization of the error Δh_c between the shape of the loading curves depicted by Bernhardt's law and the actual shape of the experimental indentation curves. This minimization is done using a set of indentation curves and reduces the scatter of the loading curves. Thus, a mean behavior is assumed for the examined material, even though it is analyzed with a local test (only a small amount of material is deformed).

Whatever the studied material (AISI 316L stainless steel, aluminum-based AU4G alloy or titanium-based Ti–6Al–4V alloy, MD-3P replica material), process (grinding, sandblasting, ultrasonic shot-peening) or even the indenter shape (Berkovich or cube-corner), a linear relation was identified between the root-mean-square roughness parameter S_q (or R_q for the two-dimensional measurements) and the standard deviation of the errors Δh_c. Each time, the best relation between the standard deviation of the errors Δh_c and the root-mean-square roughness parameter S_q was sought by testing different filtering conditions for the computation of S_q. Whatever the experimental conditions, the best linear relation was identified using the same filtering conditions for the computation of S_q: a Gaussian high-pass filter with a cutoff length of 15 μm when using a Berkovich indenter tip for the indentation tests and with a cutoff length of 5 μm when using a cube-corner tip.

All the obtained linear curves are depicted in Fig. 2. Whatever the material or surface treatment, the experimental data were well fitted with a linear relation: The coefficients of determination are all comprised between 0.9378 and 0.9979. The issue is that this linear relation has no justifications other than its reproducibility whatever the examined material, surface treatment or indenter shape. The slopes and intercepts of the regression lines are different; thus, it would seem that they are dependent on the material properties but this does not seem to be the main explanation of these relations.

It might be assumed that this relation is easy to understand because the multiple indents may be seen as the discretized results given by a tactile profilometer causing plastic deformations. The first point of the curve is recorded when a minimum stiffness is reached; thus, roughness can cause a shift of the zero-point of the indentation curves (depending on whether the indentation test is performed on summits or dales). Figure 3 schematically depicts the indentation curves obtained depending on the characteristics of surface roughness. Three main cases can be identified:

- In the first case, the size of the imprint is very small compared to the roughness wavelength. In this case, whatever the roughness amplitude,
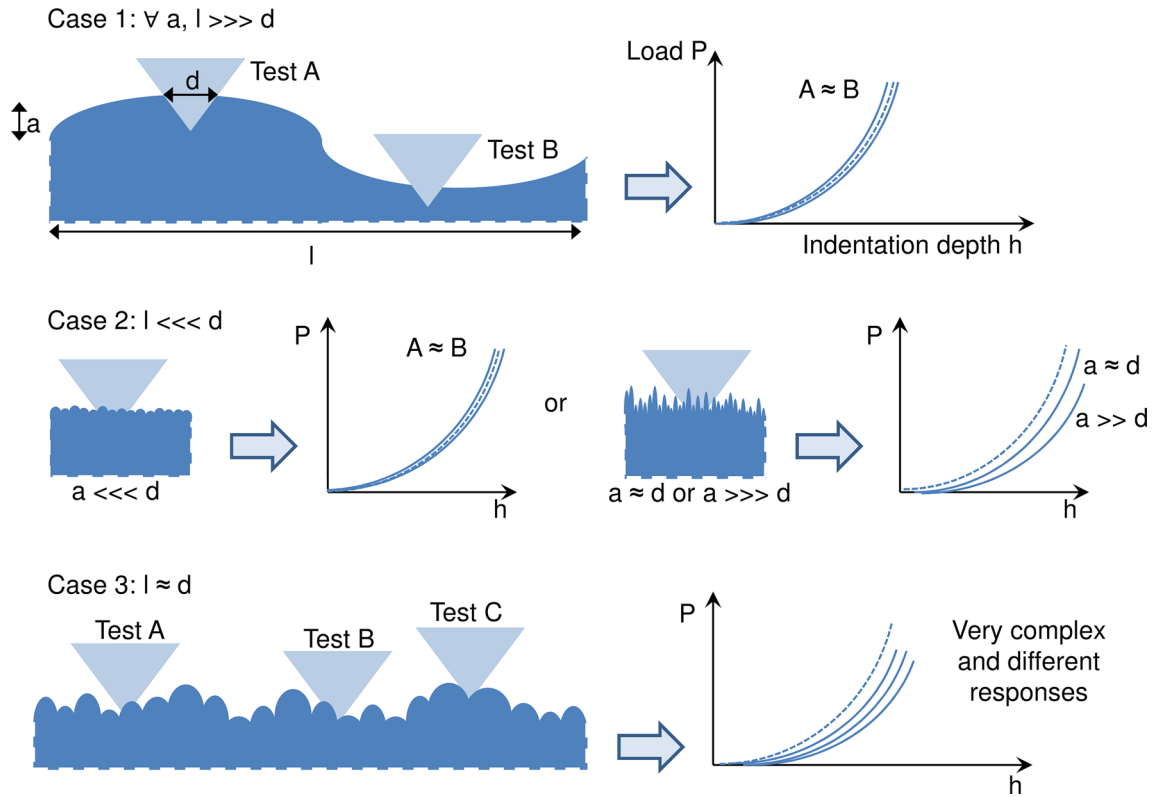
Figure 3 Schematic cases of indentation tests depending on the size of the indentation imprint (d) and the amplitude (a) and wavelength (l) of surface roughness.

indentation test results are not impacted by roughness. The wavelength of roughness is so large that it is similar to indenting a plane.

- In the second case, the size of the imprint is very large compared to the roughness wavelength. Two main subcases can then be identified. In the first one, the roughness amplitude is significantly smaller than the size of the indentation imprint; thus, roughness can be neglected. The obtained indentation curves are fairly similar. In the second subcase, the roughness amplitude is either of the same order of magnitude or larger than the size of the indentation imprint; thus, a significant scatter of the load–displacement curves is observed.
- In the third case, the roughness wavelength and the size of the indentation imprint are of the same order of magnitude. The indentation results are thus strongly impacted by roughness. However, describing the phenomena that take place is complex because depending on the roughness amplitude and the indent location, many different configurations can be obtained: As an example, increasing the roughness amplitude decreases

multi-contact. This case corresponds to the present study.

Figure 3 depicts that whatever the roughness morphology, the indentation curves begin at the origin: Only the shape of the curves change (and thus the computed hardness). The indented rough specimen is seen as a material having porous surface, and thus, for a given indentation depth, the obtained indentation curves are different. What does the minimization of the error Δh_c between the shape of the loading curves predicted by Bernhardt's law and the actual shape of the experimental curves mean in the proposed methodology? It is important to note that the macrohardness H_0 and the ISE coefficient β are determined for a set of curves. Contrary to usual treatments that determine one value of macrohardness per curve and then average the results, here, the set of curves is treated simultaneously as a whole in order to identify the value of macrohardness. The minimization of the error between the shape of the loading curves and the shape predicted by Bernhardt's law thus leads to a "shift" of the curves,

Figure 4 Indentation curve obtained with the semi-analytical model for the indentation of a smooth material (*blue round dots*), its fit with Kick's law (*blue line*) and the fitting error (*red square dots*).
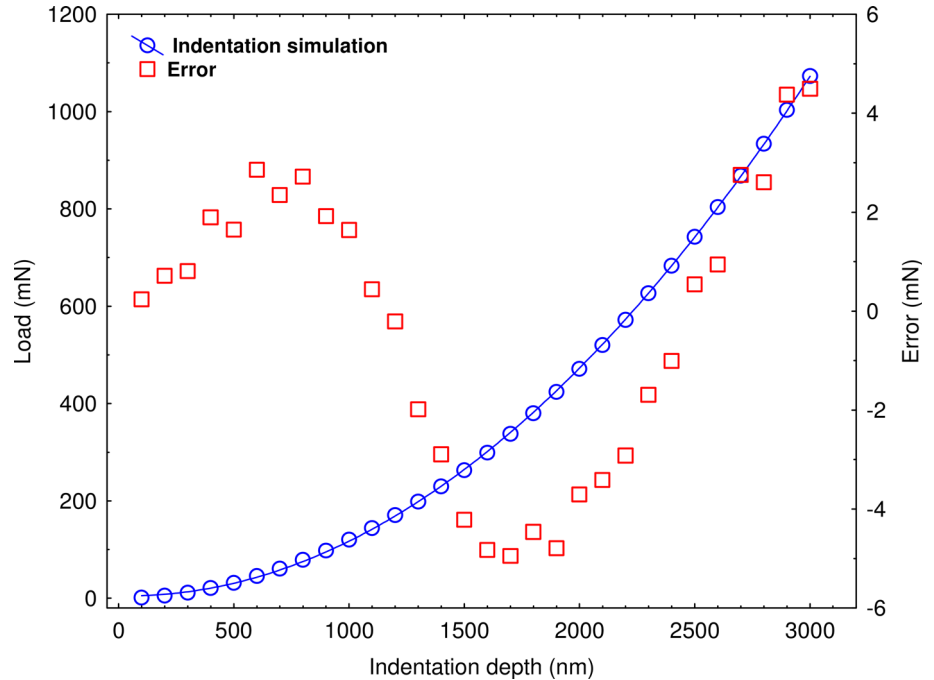
which may correspond to a compensation of the lack of matter (i.e., surface porosity) caused by surface roughness.

In order to confirm this interpretation of the experimental data, the indentation testing of a rough surface is simulated. This will enable the material parameters to be perfectly controlled and thus to answer the following questions:

- Is the scatter of the indentation curves only caused by topography or is part of it caused by the heterogeneity of the material properties?
- Can the errors between the shape of the loading curves predicted by Bernhardt's law and the actual shape of the curves be seen as a false detection of the surface by the indenter, thus giving false origins to the indentation curves?
- Is the macrohardness identified with the methodology the true material macrohardness?
- Is the use of a linear relation between the root-mean-square roughness parameter and the standard deviation of the errors Δh_c valid (see Fig. 2)?

In order to get a robust estimation and a proper description of roughness, numerical simulations of the indentation tests with pavements of 256×256 are required. Using finite element simulations would be too time-consuming because numerous indentation curves are needed and thus many numerical simulations must be performed. Therefore, the semi-

analytical model based on several hypotheses of contact mechanics, which is described in "Semi-analytical model for numerical simulation" section, is used.

Semi-analytical model results

The semi-analytical model described in "Semi-analytical model for numerical simulation" section is used to simulate the indentation of rough surfaces of titanium alloy Ti–6Al–4V specimens ground with different grit papers. The obtained numerical indentation curves are then treated using the methodology based on the minimization of the errors between the shape of the loading curves predicted by Bernhardt's law and the actual shape of the indentation curves. However, in order to simplify the study and focus on the meaning of the error Δh_c, the ISE coefficient β is set to zero for the treatment of the indentation curves obtained with the semi-analytical model. Thus, the shape of the numerical curves will be compared to the shape of a simple quadratic curve: Kick's law [19].

Validation of the semi-analytical model results: smooth surface

Before applying the model described in "Semi-analytical model for numerical simulation" section to rough specimens, it is first checked using a smooth
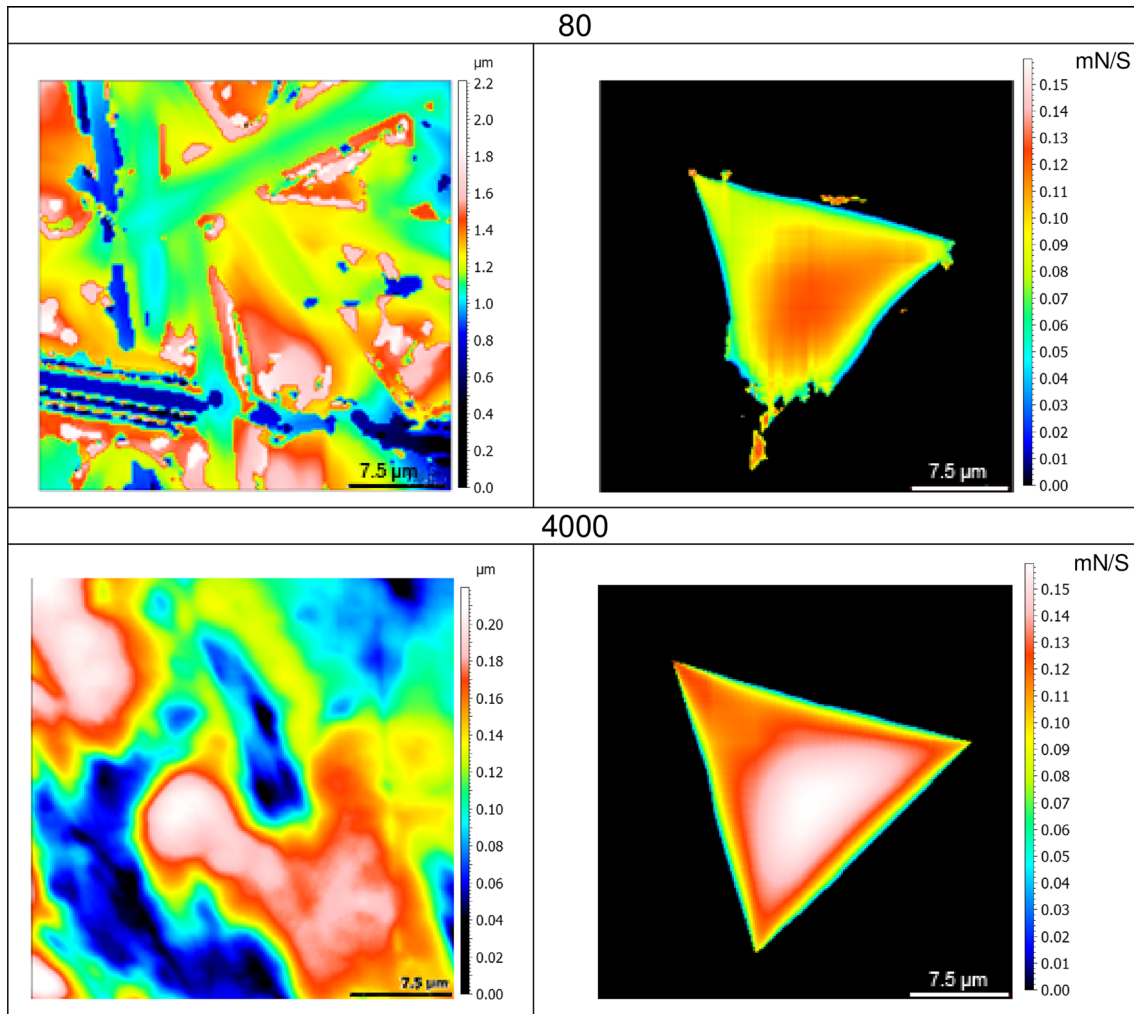
Figure 5 Examples of experimental rough surfaces, corresponding to the specimens polished with grit paper 80 and 4000 and the obtained numerical indentation imprints on these surfaces (values are contact forces in mN on each discretized cell S).

surface. The numerical simulation is checked using a smooth surface having properties similar to titanium alloy Ti–6Al–4V specimens: Its Young's modulus E is equal to 110 GPa, its Poisson's coefficient is equal to 0.3, and its elastic limit is equal to 1050 MPa. Figure 4 shows the results of this numerical simulation. The obtained load–displacement curve, represented with round blue dots, is fitted with Kick's law (which assumes that the load is proportional to the displacement raised to the power of 2), and the fitting error is displayed with red square dots. A really good fit is obtained: The load error remains lower than 10 mN on the whole curve. The identified macrohardness H_0 is equal to 4.8358 ± 0.005 GPa. The numerical simulation of the indentation test correctly reproduces real indentation test results.

Semi-analytical model applied to rough surfaces

Now, the semi-analytical model of the indentation test is used with "real" surfaces, i.e., with the three-dimensional roughness measurements taken on the eleven Ti–6Al–4V specimens ground with different grit papers used in the simulation. Figure 5 shows some examples of these rough surfaces, corresponding to the specimens polished with grit paper 80 or 4000 and the indentation imprints on these surfaces with the simulation. Some discretization issues can be observed on the numerical rough surfaces and more particularly on the smoother surfaces. It comes from the limited definitions of the roughness measurements taken with the objective $\times 20$ of the optical profilometer. A resampling is performed to limit the influence of this discretization issue.

Figure 6 Indentation curves obtained with **a** the experimental testing of Ti–6Al–4V specimens polished with different grit sizes and **b** with the semi-analytical model of the indentation testing of Ti–6Al–4V specimens polished with different grit sizes.
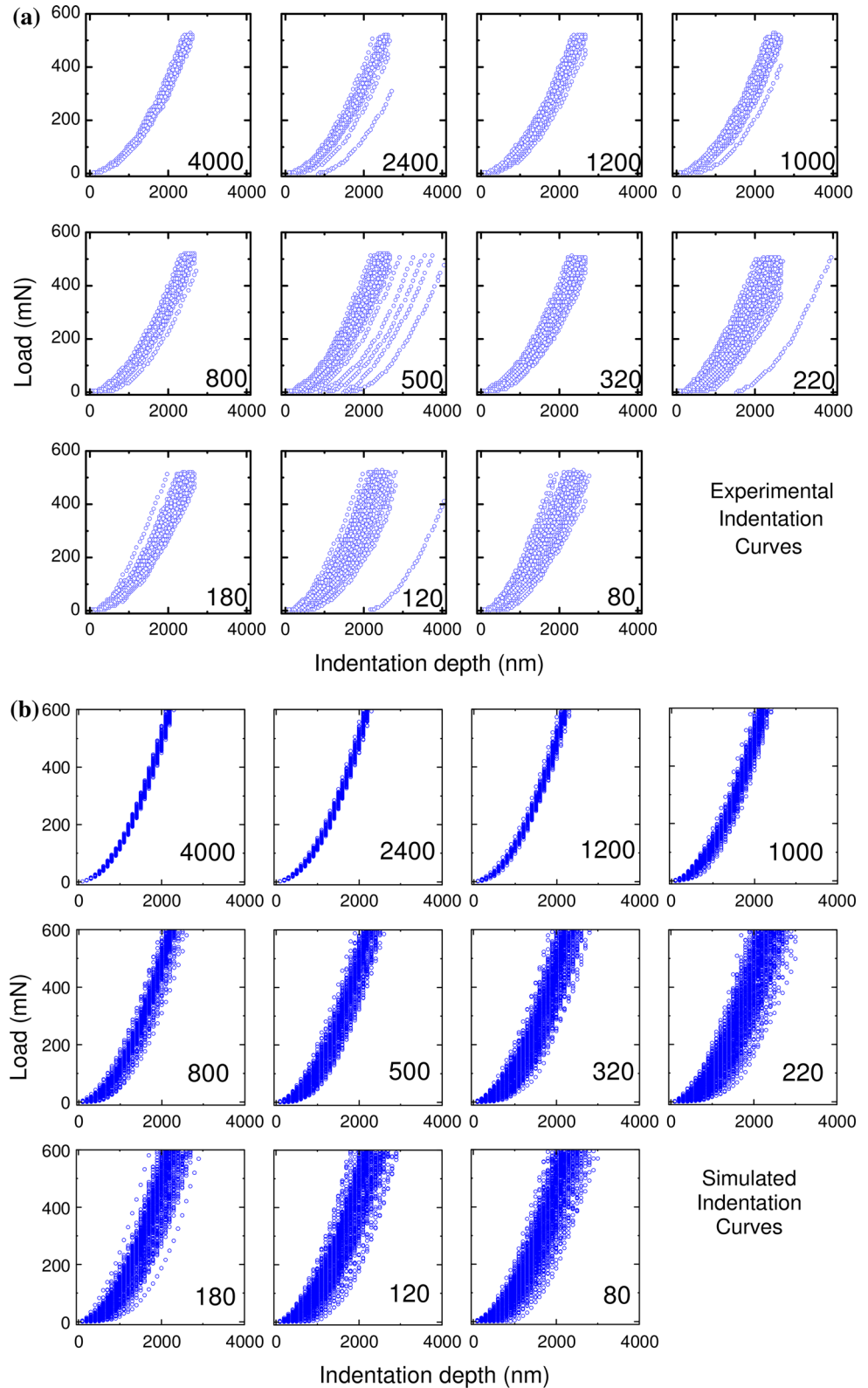
A total of 270 indentation tests were simulated for each specimen. Figure 6 shows the previously obtained experimental indentation curves for all the specimens (Fig. 6a) and those given by the numerical simulation (Fig. 6b). For the experimental and numerical indentation curves, the scatter is larger

Figure 7 Application of the methodology to **a** the experimental indentation curves of the Ti–6Al–4V specimens polished with different grit sizes **b** the indentation curves obtained with the semi-analytical model for Ti–6Al–4V specimens polished with different grit sizes.
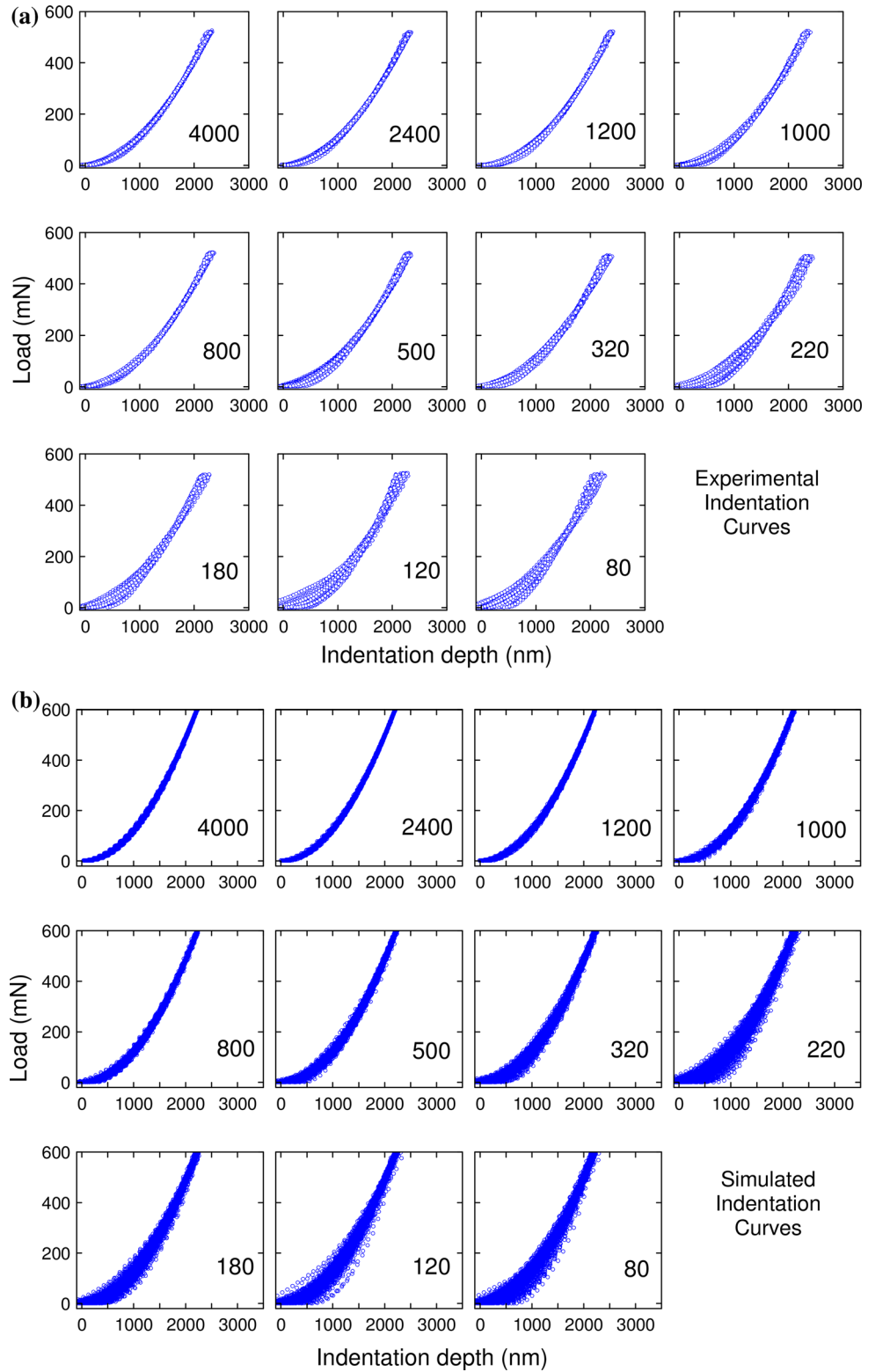

with the use of coarser particles for grinding, i.e., for rougher surfaces. Similar orders of magnitudes are found for the scatter of the curves. Figure 7 shows the application of the previously described methodology to the experimental and numerical indentation curves. This methodology enables the scatter of the

curves to be significantly decreased for all the specimens. For the experimental and numerical curves, the best results are obtained for the smoother specimens for which the indentation curves are difficult to distinguish. Similar orders of magnitudes are obtained for the correction of the experimental and numerical curves.

Figure 8 shows the distributions of the errors Δh_c between the shape of the numerical curves and the shape predicted by Bernhardt's law, in which the ISE coefficient β is equal to zero (which is equivalent to considering Kick's law). The standard deviations of the errors Δh_c reduces with the decrease of roughness. This trend is consistent with the experimental data. Only the specimen polished with paper grit 220 deviates from this trend: It shows an increase of the standard deviation compared to specimen 180. However, the same difference was observed when treating the experimental results.

Figure 9 shows the median values of the macrohardness H_0 identified with the proposed methodology and the corresponding confidence intervals for all the numerical specimens. The confidence intervals of the macrohardness increase with the increase of roughness. The median values of the macrohardness H_0 are fairly constant: Only specimen 220 has a significantly smaller macrohardness value. According to the given confidence intervals, for grit sizes lower than 800, the macrohardness values computed with the semi-analytical model show differences that can be significant. These differences cannot be due to the material behavior as it is assumed to be perfectly plastic. This means that the differences of macrohardness values are probably caused by the determination of the contact area. However, it should be noted that the absolute difference of the macrohardness values between specimen 80 and specimen 4000 is lower than 1%. Thus, the developed methodology
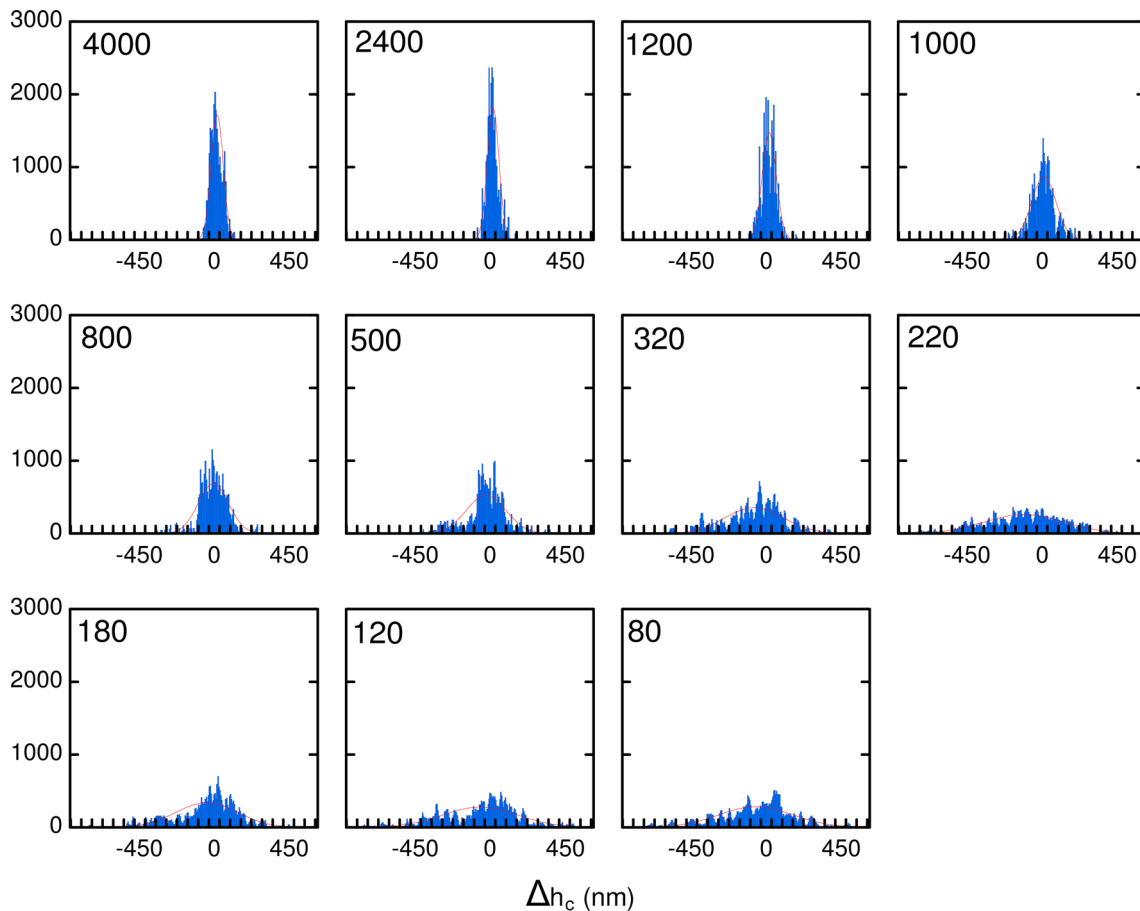
Figure 8 Distributions of the errors Δh_c between the shape of the numerical curve and the shape predicted by Bernhardt's law (when considering an ISE coefficient β equal to zero).

Figure 9 Median values of the macrohardness H_0 identified with the proposed methodology and the corresponding confidence intervals computed with the semi-analytical model for Ti–6Al–4V specimens polished with different grit sizes. The grit sizes are used as specimen names.
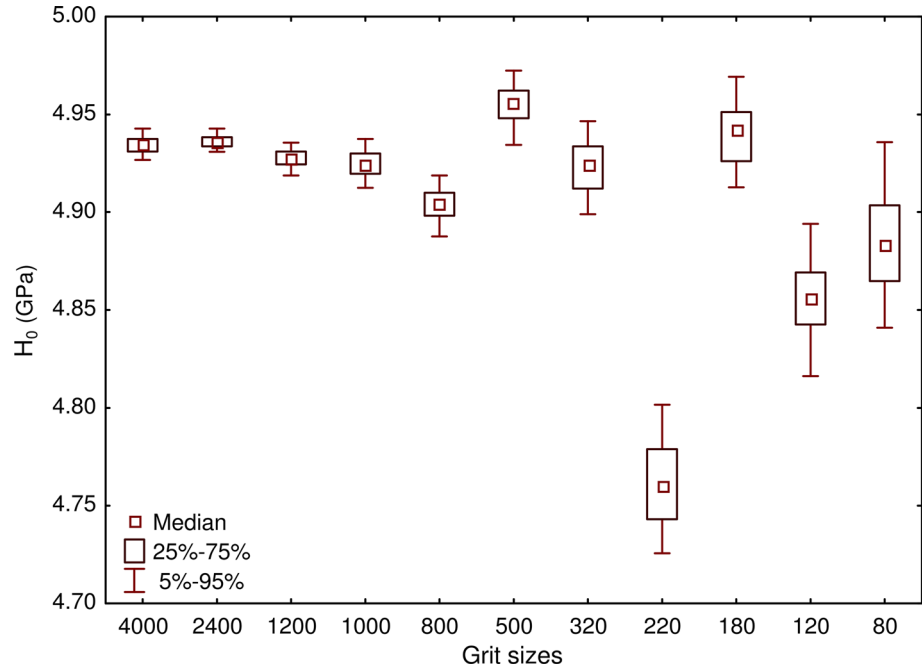
enables to accurately determine the macrohardness despite non-negligible roughness.

As previously explained in "Previously found results" section, experiments made with different materials, processes or indenters enabled us to identify a linear relation between the standard deviations of the errors Δh_c between the shape of the numerical curves and the shape predicted by Bernhardt's law and the root-mean-square roughness S_q. The approach to identifying the scale at which the best linear relation is obtained is summarized in Fig. 10. Several relationships were tested with different filtering to compute S_q. Using the experimental results, it was shown that the best linear relations between the standard deviations of the errors Δh_c between the shape of the numerical loading curves and the shape predicted by Bernhardt's law and the root-mean-square roughness S_q were obtained when using a Gaussian high-pass filter with a cutoff length value around 15 μm when using a Berkovich indenter and around 5 μm when using a cube-corner indenter. As an example, Fig. 11 shows the values of the coefficient of determination R^2 of the tested linear relations between the standard deviations of the errors Δh_c calculated with the experimental curves and the root-mean-square roughness S_q as a function of the filtering length, with (a) a Berkovich indenter and (b) a cube-corner indenter for the titanium alloy ground with different

grit papers. The cutoff length values are different according to the tested indenter shape. It thus seems that the cutoff length value is dependent on the final size of the imprint. The best relation between the standard deviation of the errors Δh_c and the root-mean-square roughness S_q was sought for the numerical indentation curves as well, by testing several cutoff lengths and filtering for the computation of S_q. The best linear relation for the numerical results was found with the use of a Gaussian high-pass filter with a cutoff length approximately equal to 15 μm. Thus, for the Berkovich indenter, the identified scale is in agreement with the experimental results.

Figure 12 shows the obtained linear relations between the standard deviation of the errors Δh_c and the root-mean-square roughness S_q computed at the relevant scale, for (a) the experimental indentation curves and (b) the numerical curves obtained with specimens of Ti–6Al–4V ground with different grit sizes. Both graphs have high values of coefficient of determination, but different regression lines are obtained. The y-intercept is equal to zero for the numerical curves and is equal to 30 nm for the experimental results. This indicates that even if the root-mean-square roughness is equal to zero, the curves need to be shifted: The zero-point of the curve is not accurately defined by the nanoindentation device. It should be noted that the indenter tip defect
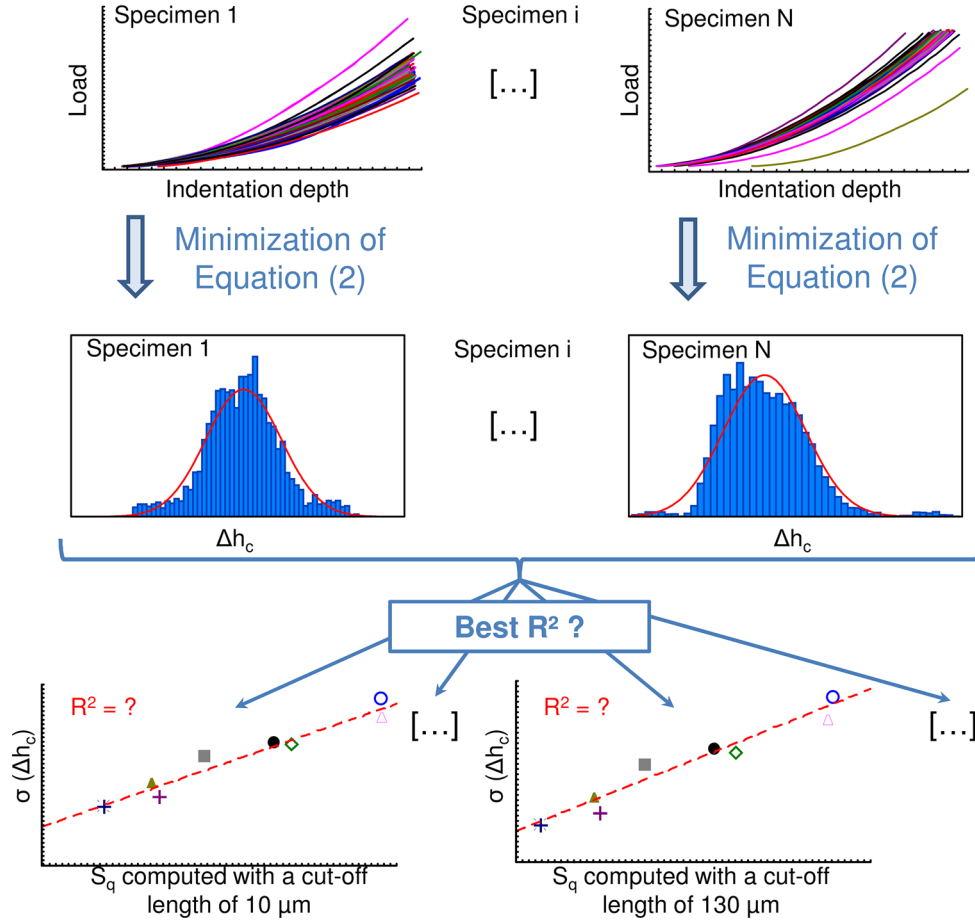
Figure 10 Diagram summarizing the approach followed in order to identify the scale at which the best linear relation between the experimental standard deviation of the errors Δh_c and the root-mean-square roughness S_q is obtained.

is not mentioned in the treatment of the experimental curves. The indenter tip defect may be thought to be the cause of the value of the y-intercept of the experimental curves. In practice, a real indenter tip is never perfectly sharp. Several authors [20, 21] suggested that the function of area of a Berkovich tip A_T should be written as:

$$A_T = 24.56(h_c + h_d)^2, \qquad (8)$$

where h_d is the blunting distance, i.e., the distance between the actual rounded tip of the indenter and the sharp end of a perfect indenter. This expression is very similar to the one used in our computation when we introduced Δh_c. The introduction of Δh_c and its minimization should correct the tip effect. Thus, the tip effect should not be the cause of the differences of y-intercepts.

The slopes identified in Fig. 12 are also different. The slope of the relation identified for the numerical curves is equal to 1.5, which is approximately three times the slope found with the experimental data (equal to 0.5). As the values of the root-mean-square roughness S_q are equal (the same surfaces are used), the slope change is caused by the shift of the curves. The identified variability of the indentation curves is larger with the semi-analytical model, compared to the experimentation. Four hypotheses can be made to explain the slope change. First, experimental data may be noisier than numerical data and thus tend to modify the slope. This is highly plausible, but cannot be quantified. Second, the discretization of roughness used for the semi-analytical model may partly explain the change of slope. This effect was checked and found to be unlikely to be true as its effect

Figure 11 Coefficient of determination R^2 of the tested relation between the experimental standard deviation of the errors Δh_c and the root-mean-square roughness S_q as a function of the cutoff length, with a **a** Berkovich indenter and **b** cube-corner indenter.
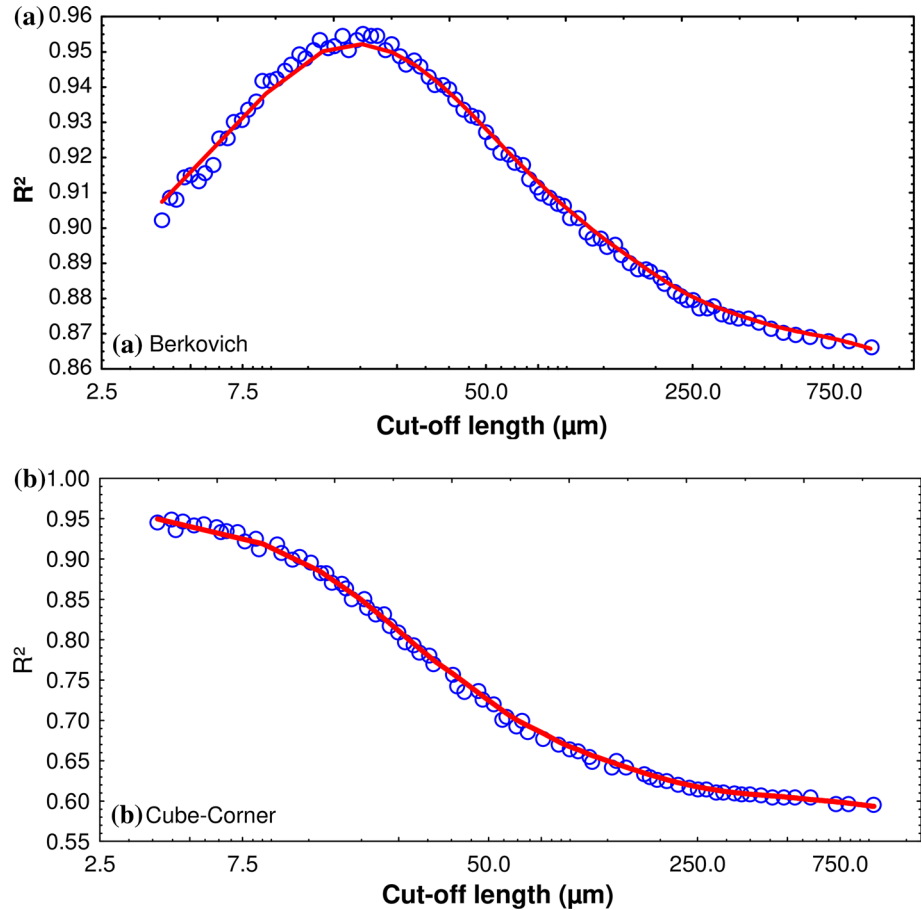

should be so small as to be negligible. Third, the detection of the first-contact may have an impact on the shifting of the curves and thus on the identified standard deviation of the errors Δh_c. Finally, abrasion debris may offer little resistance to indentation and thus may less disturb the indentation test in reality than predicted with the semi-analytical model. The third and four hypotheses are hereafter discussed in more detail.

It should be noted that, in the experiment, the load–displacement curves only start to be recorded when the stiffness is larger than 200 N m^{-1}. As there is no such condition in the semi-analytical model used to compute the numerical curves, the experimental curves can be seen as truncated compared to the experimental ones. By testing the results, it was found that truncating the curves in the experimental data leads to a decrease of the standard deviations of the errors Δh_c for particularly rough specimens. Truncating was found to have no effects on the results of specimen 4000, whereas it has a non-negligible effect on specimen 80. A similar trend is

shown in Fig. 12: The values of the standard deviations of the errors Δh_c are nearly identical for specimen 4000. Then, for grit sizes smaller than 800, the values of the standard deviations of the errors Δh_c obtained with the numerical curves are 1.5 times higher than what is obtained with the experimental curves. For specimen 80, this multiplication factor reaches 2. This trend is shown in Fig. 7: The scatter of the curves is similarly reduced in the experimental and numerical curves for specimen 4000, whereas a small change of shape can be detected from specimen 500 to specimen 80. The truncation of the curves in the experimental data can thus partly explain the slope differences. The last hypothesis assumed that abrasion debris may offer little resistance to indentation and thus may less disturb the indentation test in reality than predicted with the semi-analytical model. There are two aspects in this hypothesis. First, this effect implies that the difference of material behavior between the experimental and numerical data leads to the differences of slope identified in Fig. 12. However, it is shown in Fig. 2 that testing

Figure 12 Standard deviation of the errors Δh_c as a function of the root-mean-square roughness S_q computed with a high-pass filter and a cutoff length equal to 15 µm, using **a** the experimental results of the Ti–6Al–4V specimens polished with different grit sizes and **b** the numerical indentation curves.
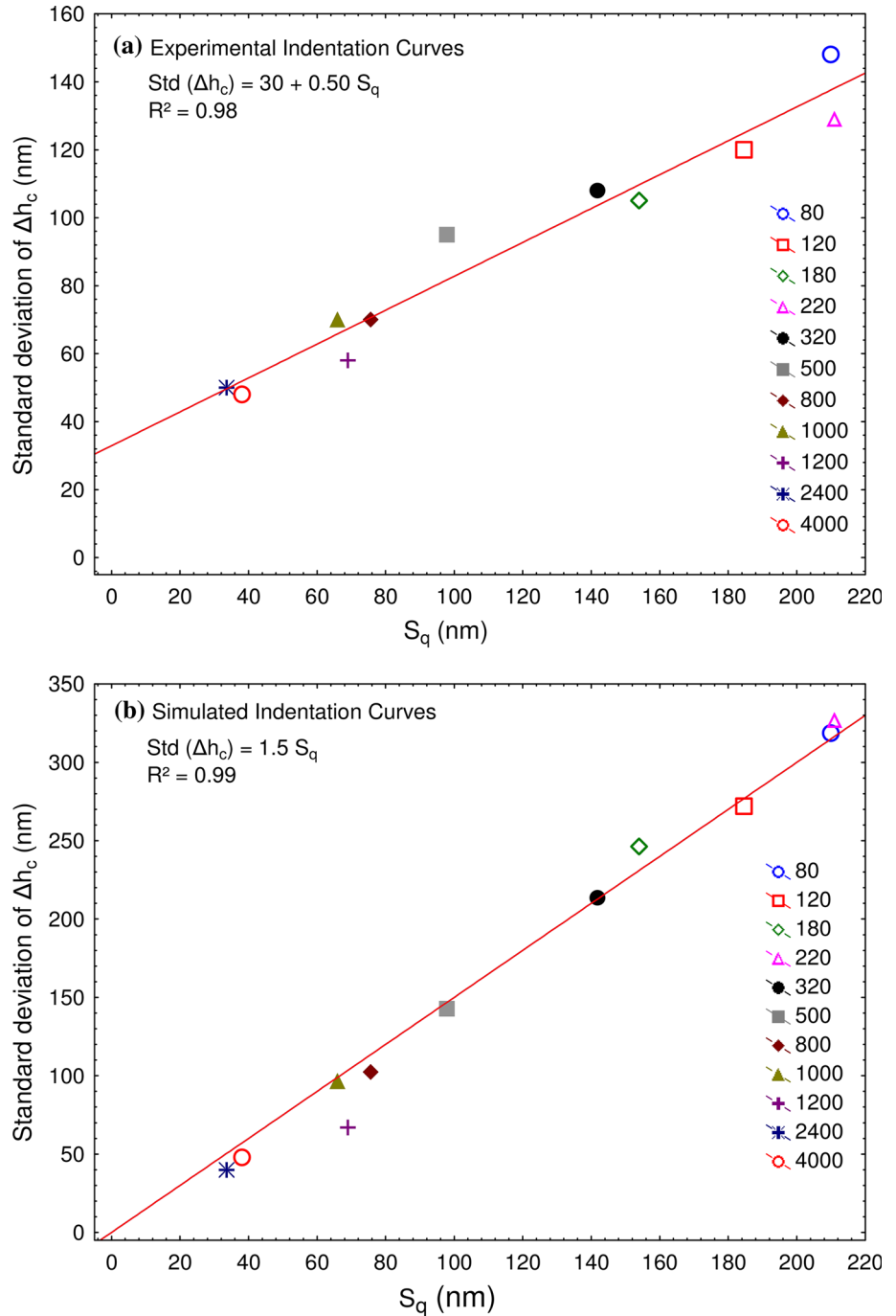
similar morphologies with different materials leads to identify similar slopes. As an example, a slope approximately equal to 0.66 was identified for the MD-3P material used to produce replicas of the polished Ti–6Al–4V specimens. Nevertheless, the numerical simulation may overestimate the debris resistance, but further testing is required to test this hypothesis.

Despite the slope differences, applying the methodology to the indentation curves obtained with the semi-analytical model led to underlining the importance of the choice of the scale at which roughness is computed. Indeed, both the experimental and numerical indentation curves led to the identification of a specific scale: The best relation between the errors between the shape of the

numerical curves and the shape predicted by Bernhardt's law and the root-mean-square roughness S_q is obtained when using a high-pass filter with a cutoff length of 15 μm. This scale corresponds to the order of magnitude of the indentation imprint size. Therefore, in order to be relevantly considered, roughness must be filtered at the scale of the phenomena, which is in this case at the size of the indentation imprints.

Conclusion

A semi-analytical model was used in order to validate the results found using a previously developed methodology of treatment of indentation curves for the identification of mechanical properties despite significant roughness. Despite the simplicity of the semi-analytical model, the results obtained with the semi-analytical model and the experimental results obtained by testing Ti–6Al–4V specimens ground with different grit sizes showed good agreement. For the experimental and numerical indentation curves, the scatter is larger for rougher surfaces. Similar orders of magnitude are found for the scatter of the curves and the values of macrohardness identified with the methodology. The numerical results also permitted us to identify a relationship between the standard deviation of the errors Δh_c between the shape of the numerical curves and the shape predicted by Bernhardt's law and the root-mean-square roughness S_q. The best relation was found when computing the S_q parameter with a Gaussian high-pass filter with a cutoff length of 15 μm, thus confirming the experimental results. This scale corresponds to the size of the indentation imprints. Thus, the relevant examination of the effect of roughness on indentation testing requires the filtering of the roughness parameters at the scale of contact, i.e., at the scale of the indentation imprints.

However, the slopes and y-intercepts of the relationship identified using the numerical and experimental results are different. The y-intercept found with the numerical curves is equal to zero contrary to the one identified with the experimental curves, which is equal to 30 nm. This indicates that even if S_q is equal to zero, the zero-point of the curve is not accurately determined by the instrumented indentation device. As for the slope differences, it may be partly due to experimental noise and the differences of methodology of detections of first-contact for the

recording of the load–displacement curves. Overestimation of the resistance of abrasion debris by the semi-analytical model may also explain the differences of slopes. However, further testing is required to confirm this hypothesis.

Compliance with ethical standards

Conflict of interest The authors declare that they have no conflict of interest.

References

[1] Bobji MS, Shivakumar K, Alehossein H, Venkateshwarlu V, Biswas SK (1999) Influence of surface roughness on the scatter in hardness measurements—a numerical study. Int J Rock Mech Min Sci 36(3):399–404

[2] Walter C, Antretter T, Daniel R, Mitterer C (2007) Finite element simulation of the effect of surface roughness on nanoindentation of thin films with spherical indenters. Surf Coat Technol 202(4–7):1103–1107

[3] Qasmi M, Delobelle P (2006) Influence of the average roughness Rms on the precision of the Young's modulus and hardness determination using nanoindentation technique with a Berkovich indenter. Surf Coat Technol 201(3–4):1191–1199

[4] Kim J-Y, Kang S-K, Lee J-J, J-i Jang, Lee Y-H, Kwon D (2007) Influence of surface-roughness on indentation size effect. Acta Mater 55(10):3555–3562

[5] Guillonneau G, Kermouche G, Bec S, Loubet JL (2014) A simple method to minimize displacement measurement uncertainties using dynamic nanoindentation testing. Tribol Int 70:190–198. doi:10.1016/j.triboint.2013.10.013

[6] Marteau J, Bigerelle M, Xia Y, Mazeran PE, Bouvier S (2013) Quantification of first contact detection errors on hardness and indentation size effect measurements. Tribol Int 59:154–162. doi:10.1016/j.triboint.2012.06.029

[7] Standardization IOf (1997) NF EN ISO 4287 Spécification géométrique des produits (GPS)—État de surface: méthode du profil—Termes, définitions et paramètres d'état de surface. vol International Organization for Standardization,

[8] Standardization IOf (1998) NF EN ISO 4288 Spécification géométrique des produits (GPS)—État de surface: méthode du profil—Règles et procédures pour l'évaluation de l'état de surface. vol International Organization for Standardization,

[9] Bernhardt EO (1941) On microhardness of solids at the limit of Kick's similarity law. Z Metallkd 33:135–144

[10] Xia Y, Bigerelle M, Marteau J, Mazeran PE, Bouvier S, Iost A (2013) Effect of surface roughness in the determination of the mechanical properties of material using nanoindentation test. Scanning 36(1):134–149

[11] Marteau J, Bigerelle M (2015) Relation between surface hardening and roughness induced by ultrasonic shot peening. Tribol Int 83:105–113

[12] Ho SH, Xia Y, Marteau J, Bigerelle M (2013) Influence de l'amplitude de la rugosité de surfaces sablées sur la mesure de dureté par nanoindentation. Mat Tech 101:305–314. doi:10.1051/mattech/2013070

[13] Xia Y, Bigerelle M, Bouvier S, Iost A, Mazeran PE (2015) Quantitative approach to determine the mechanical properties by nanoindentation test: application on sandblasted materials. Tribol Int 82(B):297–304. doi:10.1016/j.triboint.2014.07.022

[14] Marteau J, Wieczorowski M, Xia Y, Bigerelle M (2014) Multiscale assessment of the accuracy of surface replication. Surf Topogr Metrol Prop 2(4):044002. doi:10.1088/2051-672X/2/4/044002

[15] Marteau J, Mazeran PE, Bouvier S, Bigerelle M (2012) Zero-point correction method for nanoindentation tests to accurately quantify hardness and indentation size effect. Strain 48(6):491–497. doi:10.1111/j.1475-1305.2012.00846.x

[16] Oliver WC, Pharr GM (1992) An improved technique for determining hardness and elastic modulus using load and displacement sensing indentation experiments. J Mater Res 7(06):1564–1583

[17] Johnson KL (1985) Contact mechanics. Cambridge University Press, London

[18] Jourani A, Dursapt M, Hamdi H, Rech J, Zahouani H (2005) Effect of the belt grinding on the surface texture: modeling of the contact and abrasive wear. Wear 259(7–12):1137–1143. doi:10.1016/j.wear.2005.02.113

[19] Kick F (1885) Das Gesetz der proportionalen Widerstände und seine Anwendungen: Nebst Versuchen über das Verhalten verschiedener Materialien bei gleichen Formänderungen sowohl unter der Presse als dem Schlagwerk. Verlag von Arthur Felix, Leipzig, Germany

[20] Bull SJ, Page TF, Yoffe EH (1989) An explanation of the indentation size effect in ceramics. Philos Mag Lett 59(6):281–288. doi:10.1080/09500838908206356

[21] Gong J, Miao H, Peng Z (2004) On the contact area for nanoindentation tests with Berkovich indenter: case study on soda-lime glass. Mater Lett 58(7–8):1349–1353. doi:10.1016/j.matlet.2003.09.026